University of Sistan and Baluchestan

Challenges in Nano and Micro Scale Science and Technology

Online ISSN: 2821 - 000X

A Simulation Study of Forced, Free, and Mixed Convection of Al_2O_3-Water Nanofluid Flow Inside a Cavity

Tohid Adibi

Department of Mechanical Engineering, University of Bonab, Bonab, Iran. E-mail: Tohidadibi@ubonab.ac.ir

Article Info

Article type:
Research Article

Article history:
Received: 31 March 2026
Received in revised form: 09 April 2026
Accepted: 24 April 2026

Keywords:
Nanofluid convection,
Al_2O_3–water
Cavity flow,
Global energy efficiency
TEC/TEP,
Grid-independence and convergence

ABSTRACT

Purpose: This study aims to investigate the heat transfer and fluid flow characteristics of alumina (Al_2O_3) based nanofluids under various convective conditions, with a particular focus on understanding the interplay between thermal performance and hydrodynamic costs. The primary goal is to elucidate the innovative aspect of using nanofluids in different flow regimes, addressing a fundamental question regarding their efficiency.

Methodology: A numerical simulation approach was employed to analyze the behavior of the nanofluid. The simulations were conducted under specific boundary conditions, including a cold, rightward-moving top plate and a hot, leftward-moving bottom plate. The side walls were treated as adiabatic. The nanofluid, containing 5% by volume of Al_2O_3 nanoparticles, was modeled considering both forced convection due to the moving plates and natural convection driven by temperature differences. The Richardson number, representing the ratio of natural to forced convection, was systematically varied to cover a wide range of flow regimes.

Main Findings: This study numerically investigates the thermofluid performance of Al_2O_3–water nanofluid (5% vol.) in a cavity across forced (Ri=0.1), mixed (Ri=1), and natural (Ri=10) convection regimes. While heat transfer shows modest gains (Nu increases from 13.67 to 13.77 at Ri=0.1, and 14.78 to 16.23 at Ri=1), the friction factor significantly rises (e.g., from 1.31 to 2.39 at Ri=0.1). The Thermally Enhanced Performance (TEP) index consistently remains below unity (approx. 0.82-0.84), indicating that increased viscous resistance outweighs thermal benefits. Consequently, the Al_2O_3–water nanofluid does not enhance overall system energy efficiency under the studied conditions, highlighting the need for holistic performance assessment in engineering applications.

NOMENCLATURE

A	Area	Pr	Prandtl number
C	The volume fraction of nanoparticle	u, v	X, y velocity components
C_p	Specific heat in constant pressure (J/kg/K)	t	Time
f	Friction factor	U, v	Velocities
$\bar{f}$	Mean friction factor	x, y, r	Coordinates
Gr	Grashof number	**Greek symbols**	
k	Thermal conductivity (W/m/K)	β	Thermal expansion coefficient (K^{-1})
M	Number of cells in x-direction	μ	Coefficient of viscosity (kg/m/s)
N	Number of cells in y-direction	ω	Rotational speed
Nc	Thermal conductivity parameter	υ	Kinematic viscosity (m^2/s)
Nu	Local Nusselt number	ρ	Density (kg/m^3)
$\overline{Nu}$	Mean Nusselt number	τ	Shear stress
Nv	Dynamic viscous parameter	∈	Artificial compressibility

How to Cite this paper: Adibi T. A Simulation Study of Forced, Free, and Mixed Convection of Al_2O_3-Water Nanofluid Flow Inside a Cavity. *Challenges in Nano and Micro Scale Science and Technology*. 2026; 14(1): 10-20. DOI: 10.22111/cnmst.2026.55024.1289

 Publisher: University of Sistan and Baluchestan.
DOI: 10.22111/cnmst.2026.55024.1289

P	Pressure	**Subscripts**	
Re	Reynolds number	ref	Reference
Ri	Richardson	bf	Body fluid
T	Temperature	nf	Nano-fluid
		p	Particle

1. INTRODUCTION

Driven by the increasing demand for efficient cooling systems[1, 2], the utilization of nanofluids as a novel approach in heat transfer has gained considerable attention[3-6]. Consequently, investigating the behavior of nanofluids under various flow conditions, including forced, free, and mixed convection, is of paramount importance[7-9]. This paper presents a numerical and simulation-based study of the behavior of Al2O3-Water nanofluid within a cavity, considering different flow regimes.

Addressing air pollution[10-12], global warming[13, 14], and environmental concerns, alongside reducing associated costs, necessitates the optimization of thermal systems[15, 16] and the integration of renewable energy sources. Enhancing heat transfer is a fundamental aspect of this optimization[17, 18]. Heat transfer enhancement techniques are broadly classified into active and passive methods [19]. Active methods utilize external energy sources, such as electric or magnetic fields, or acoustic forces, to manipulate fluid flow and boost heat transfer rates. Conversely, passive methods achieve enhancement through modifications to the system's geometry or alterations to the working fluid [20]. Nanofluids, representing a relatively recent class of working fluids, fall under the category of passive methods. These are defined as stable suspensions of nano-sized particles within a base fluid. Due to the typically higher thermal conductivity of solid materials compared to conventional fluids, the incorporation of these particles can significantly improve thermal properties[21]. The promising characteristics of nanofluids have spurred considerable research and engineering efforts exploring their application in diverse fields, including micro electro-mechanical systems (MEMS), fuel cells, and metal heat treatment [22]. While a robust experimental database is crucial for developing a comprehensive theoretical understanding of nanofluids, conducting such research presents significant challenges. Experimental investigations are often expensive and time-consuming[23, 24], and working with nanoparticles can pose safety risks. Furthermore, obtaining precise data can be difficult, particularly when measuring temperatures at specific points within micro-channels[25, 26]. Measurement instrument uncertainties and potential errors—instrumental, environmental, procedural, and human—further complicate experimental approaches[25, 27]. Numerical methods, however, offer a powerful alternative for analyzing physical phenomena, providing detailed insights at any desired location[28, 29].

Shahmohammadi and Beiki[30] numerically investigated the impact of γ-Al_2O_3 nanoparticles on heat transfer and pressure drop within the shell side of small shell-and-tube heat exchangers, operating under turbulent conditions. Using γ-Al_2O_3-water nanofluids in the shell and pure water in the tubes, the research found that both heat transfer and pressure drop increased with higher mass flow rates and more baffles. While nanoparticle addition didn't significantly affect pressure drop, the optimal heat transfer performance was achieved with a 1 vol.% nanoparticle concentration. The study also determined a suitable baffle spacing of 43.4% of the shell diameter, consistent with the Bell-Delaware method. Raei et al. [31] experimentally measured the overall heat transfer coefficient and friction factor of γ-Al_2O_3/water nanofluid in a double-tube counterflow heat exchanger under turbulent flow conditions. To ensure nanoparticle dispersion, a magnetic stirrer and ultrasonic vibrator (240 kW, 35 kHz) were used. The stabilized nanofluid, at concentrations of 0.05 and 0.15 vol.%, was tested with flow rates between 7 and 9 l/min, and inlet temperatures of 45, 55, and 65 °C. Results showed that increasing nanofluid flow rate, concentration, and inlet temperature improved both the overall heat transfer coefficient and heat transfer rate. However, the ratio of the nanofluid's heat transfer coefficient to that of pure water decreased with increasing flow rate. The maximum enhancements observed compared to distilled water were 19.3% for the heat transfer coefficient, 10% for the heat transfer rate, and 25% for the friction factor, all occurring at a concentration of 0.15. Moravej [25] experimentally investigated a novel triangular flat plate solar collector, designed and built by the author according to ASHRAE93-2010 standards. The collector, featuring a riser-less design with spiral tubes, was tested using both water and Al_2O_3-water nanofluids at concentrations of 0.1%, 0.2%, and 0.3%, and flow rates ranging from 0.0063 to 0.0378 lit/s. Performance was evaluated based on environmental factors (temperature, radiation) and thermal parameters. Results demonstrated that the triangular design, due to its geometry and reduced tube length, offers suitable performance for water heating applications. The time constant ranged from 2.5 to 4.5 minutes. Utilizing nanofluids resulted in an average efficiency increase of 12.4% compared to water, with a maximum efficiency exceeding 68.3% achieved at a 0.3% concentration and a flow rate of 0.0378 lit/s. Furthermore, the pressure drops across the collector remained minimal, below 0.1 bar.

In cavity flows involving nanofluids, most existing studies primarily report heat-transfer enhancement while overlooking the coupled influence of viscous resistance and pumping-power demand, which ultimately governs the net energy efficiency of practical thermal systems. The present work addresses this gap by examining how the interplay between buoyancy forces and forced circulation—characterized through Ri = 0.1, 1, and 10—influences both heat-transfer performance and the associated energy cost inside a closed cavity. The focus is placed on the fundamental question of whether

nanofluid-induced thermal enhancement can outweigh the hydrodynamic penalties in different convection regimes. By quantifying Nusselt number, friction factor, and energy-efficiency metrics (TEP/PEC) in a unified framework, this study provides a physics-based assessment relevant to applications such as compact cavity-based cooling units, small-scale thermal storage modules, and enclosure-type heat-management systems where both thermal and pumping demands are tightly coupled.

2. METHODS AND MATERIAL

In numerical simulations, nano-fluids are often treated as single-phase fluids, with their thermophysical properties determined by those of the base fluid and the dispersed nanoparticles. The following Navier-Stokes equations, incorporating heat transfer, govern the behavior of a two-dimensional nano-fluid[9]:

$$\begin{aligned}
&\frac{\partial u}{\partial x}+\frac{\partial v}{\partial y}=0\\
&\frac{\partial u}{\partial t}+u\frac{\partial u}{\partial x}+v\frac{\partial u}{\partial y}\\
&\qquad=-\frac{1}{\rho}\frac{\partial p}{\partial x}+\upsilon\left(\frac{\partial^2 u}{\partial x^2}\right.\\
&\qquad\left.+\frac{\partial^2 u}{\partial y^2}\right),\\
&\frac{\partial v}{\partial t}+u\frac{\partial v}{\partial x}+v\frac{\partial v}{\partial y}\\
&\qquad=-g-\frac{1}{\rho}\frac{\partial p}{\partial y}\\
&\qquad+\upsilon\left(\frac{\partial^2 v}{\partial x^2}+\frac{\partial^2 v}{\partial y^2}\right),\\
&\frac{\partial T}{\partial t}+u\frac{\partial T}{\partial x}+v\frac{\partial T}{\partial y}\\
&\qquad=\frac{1}{\rho C_p}\left(u\frac{\partial p}{\partial x}\right.\\
&\qquad\left.+v\frac{\partial p}{\partial y}\right)\\
&\qquad+\frac{k}{\rho C_p}\left(\frac{\partial^2 T}{\partial x^2}+\frac{\partial^2 T}{\partial y^2}\right)\\
&\qquad+\frac{\mu}{\rho C_p}\Phi,\\
&\Phi=\left(\frac{\partial u}{\partial y}+\frac{\partial v}{\partial x}\right)^2+2\left(\left(\frac{\partial u}{\partial x}\right)^2\right.\\
&\qquad\left.+\left(\frac{\partial v}{\partial y}\right)^2\right)
\end{aligned}\qquad (1)$$

The Chorin artificial compressibility method [32] was implemented by incorporating a pressure gradient term into the continuity equation, allowing for pressure determination through numerical solution. This modification alters the governing equations, enabling the application of a characteristics-based scheme developed by our team. This scheme effectively addresses the limitations of previous averaging schemes [33-35], specifically resolving the instability issues associated with those approaches[9].

$$\frac{1}{\varepsilon}\frac{\partial p}{\partial t}+\frac{\partial u}{\partial x}+\frac{\partial v}{\partial y}=0, \qquad (2)$$

The governing equations were transformed into dimensionless form and expressed in matrix notation as follows:[9]

$$\frac{\partial Q}{\partial t}+\frac{\partial F}{\partial x}+\frac{\partial G}{\partial y}=\frac{\partial R}{\partial x}+\frac{\partial S}{\partial y}+H$$

$$Z=\begin{bmatrix}p\\u\\v\\T\end{bmatrix},\quad F=\begin{bmatrix}\beta u\\p+u^2\\uv\\(T-Ec\,p)u\end{bmatrix},\quad G=\begin{bmatrix}\beta v\\uv\\p+v^2\\(T-Ec\,p)v\end{bmatrix},\quad R=\frac{1}{\mathrm{Re}}\begin{bmatrix}0\\\frac{\partial u}{\partial x}\\\frac{\partial v}{\partial x}\\\frac{1}{\mathrm{Pr}}\frac{\partial T}{\partial x}\end{bmatrix},$$

$$S=\frac{1}{\mathrm{Re}}\begin{bmatrix}0\\\frac{\partial u}{\partial y}\\\frac{\partial v}{\partial y}\\\frac{1}{\mathrm{Pr}}\frac{\partial T}{\partial y}\end{bmatrix},\quad H=\begin{bmatrix}0\\0\\\frac{Gr}{\mathrm{Re}^2}T\\\frac{Ec}{\mathrm{Re}}\Phi\end{bmatrix},\quad \Phi=\left(\frac{\partial u}{\partial y}+\frac{\partial v}{\partial x}\right)^2+2\left(\left(\frac{\partial u}{\partial x}\right)^2+\left(\frac{\partial v}{\partial y}\right)^2\right), \qquad (3)$$

Used dimensionless number are obtained by:

$$\begin{aligned}
&Re=\frac{\rho_{ref}u_{ref}L_{ref}}{\mu},Pr=\frac{c_P\mu}{k},\quad Ec\\
&\qquad=\frac{u_{ref}^2}{c_P\left(T_{ref2}-T_{ref1}\right)},\\
&Gr=\frac{\beta_{ex}\,g\left(T_{ref2}-T_{ref1}\right)L_{ref}^3}{\upsilon^2},Ri=\frac{Gr}{Re^2}
\end{aligned}\qquad (4)$$

The reference length for a cavity flow is the width of the cavity. The Mach number of the flow is less than 0.3, hence, the flow is considered incompressible flow, but the Boussinesq assumption is applied for density change in the y-direction because of the temperature gradient in the flow field. Reference temperatures are the temperature of warm and cold walls for cavity. The properties of water, nanoparticles, and nano-fluids are extracted from Ref. [36]. The following equations are used for nano-fluids in order to find the thermodynamically characteristics of the nano-fluid [37].

$$\begin{aligned}
&\frac{\rho_{nf}}{\rho_{bf}}=1-C+C\frac{\rho_p}{\rho_{bf}};\frac{\mu_{nf}}{\mu_{bf}}=1+CNv;\frac{(\rho C_p)_{nf}}{(\rho C_p)_{bf}}\\
&\qquad=1-C+C\frac{(\rho C_p)_p}{(\rho C_p)_{bf}};\\
&\frac{k_{nf}}{k_{bf}}=1+CNc;\frac{\beta_{nf}}{\beta_{bf}}=\frac{\rho_{nf}}{\rho_{bf}}\left[(1-C)+C\frac{(\rho\beta)_p}{(\rho\beta)_{bf}}\right].
\end{aligned}\qquad (5)$$

The governing equations were discretized using the Finite Volume Method (FVM), and a fifth-order Runge-Kutta scheme was employed for time discretization[9]

$$Z_{ijk}^{(q)}=Z_{ijk}^{(n)}-F\left(Z_{ijk}^{(q-1)}\right),\quad \alpha_q=\frac{1}{4},\frac{1}{6},\frac{3}{8},\frac{1}{2},1,\quad q=1,2,\ldots,5. \qquad (6)$$

The time step is considered 10^{-4} for a stable solution. The usual upwind scheme can be used for time discretization but the Rung-Kutta method is more stable[38, 39]. The convective fluxes are calculated by the

characteristic-based scheme introduced by ourselves [33, 34]. The first-order derivatives (convective fluxes) in cell centers are changed to normal parameters on cell boundaries by Green's theorem. A simple method to calculate the convective fluxes is the averaging method. In this method, the convective fluxes are obtained by a simple average of cell center data. But this method is not stable. So, it is replaced by a characteristics-based method that was introduced by the authors. The introduced scheme is stable. The pseudo wave propagation is considered in this method and convective fluxes are calculated by the pseudo waves. This scheme is explained with details in [33, 34]. The viscous fluxes (The second-order derivatives) in the cell center are replaced by the first-order derivatives on the cell boundaries. Obtained first-order derivatives are replaced by normal parameters on the boundaries of secondary cells by the aim of the Green theorem (equation 7)[9].

$$\left.\frac{\partial \xi}{\partial x}\right|_{AB} = \frac{1}{A}\iint_A \frac{\partial \zeta}{\partial x} ds = \frac{1}{A}\oint \zeta dy = \frac{1}{A}\sum_{k=1}^{4} \xi \Delta y_k \,, \zeta = u, v, T. \tag{7}$$

where, friction factor and Nusselt number are calculated as[9]:

$$f = \frac{2}{Re\frac{\mu_{nf}}{\mu_{bf}}\frac{\partial u}{\partial y}\frac{2}{Re\frac{\mu_{nf}}{\mu_{bf}}\frac{u_2-u_1}{y_2-y_1}\frac{2}{Re\frac{k_{nf}}{k_{bf}}\frac{\partial T}{\partial y}\frac{2}{Re\frac{k_{nf}}{k_{bf}}\frac{T_2-T_1}{y_2-y_1}}}}} \tag{8}$$

Also, mean friction factor and average Nusselt number are obtained as[9]

$$\bar{f} = \int_0^1 f dx = \frac{1}{N}\sum_{j=1}^{N} f_j \,; \bar{N}u = \int_0^1 Nu dx = \frac{1}{N}\sum_{j=1}^{N} Nu_j \,; \tag{9}$$

The top surface of the cavity is cooled and moves to the right, while the bottom surface is heated and moves to the left. The side walls are insulated and stationary. The no-slip boundary condition is applied at all boundaries, resulting in the nano-fluid velocity and temperature matching the solid boundary values. Pressure at all boundaries was determined using a second-order extrapolation method. For the initial conditions, the nano-fluid temperature and velocity were initialized to the average of the top and bottom plate temperatures and velocities, respectively. Given the use of dimensionless parameters at the boundaries, the maximum velocity and temperature are set to 1, and the minimum velocity and temperature are set to -1.

The alumina (Al_2O_3) nanoparticles used in this study have a volume fraction of **5%**. The stability of the nanofluid is a critical consideration. In this work, we assume a stable nanofluid suspension, where nanoparticles remain uniformly dispersed and do not agglomerate, which is a common assumption in many simulation studies of this nature. Factors such as surfactant addition or proper surface modification of nanoparticles are typically employed to ensure long-term stability in experimental settings, which we have implicitly considered by assuming a well-dispersed state.

3. RESULTS AND DISCUSSION

In numerical simulations, examining the convergence history is crucial for assessing the accuracy and stability of the obtained solutions. This analysis not only determines the necessary number of iterations to achieve an acceptable error level but also helps identify potential instabilities, numerical discrepancies, and the influence of model parameters (such as the Richardson number) on convergence speed. By tracking the reduction of residuals throughout the iterations, systematic adjustments to stopping criteria (e.g., error thresholds) can be made, preventing unnecessary computational expense. Therefore, presenting the convergence history in scientific publications ensures transparency in the performance of numerical algorithms and validates the final results. The error is obtained by[9]:

$$Error = \frac{\sum_{j=1}^{N}\sum_{i=1}^{M}\left(u_{i,j}^{k+1} - u_{i,j}^{k}\right)}{NM} \tag{10}$$

The convergence history of the simulations was obtained and is presented in Fig. 1. Simulations were conducted for both forced and mixed convection scenarios with Richardson numbers of 0.1 and 1. As shown in the figure, convergence in forced convection was significantly faster, reaching a residual error of 10^{-5} within 1067 iterations. In contrast, achieving the same level of accuracy (error below 10^{-5}) in mixed convection required 4580 iterations, indicating a considerably slower convergence rate.

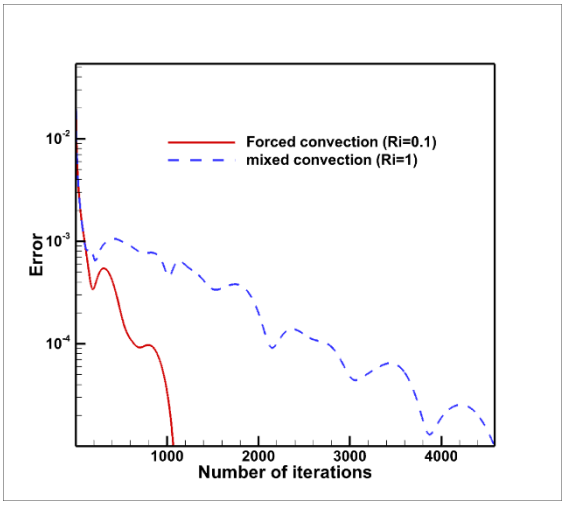

Fig. 1. comparision of forced and mixed convection convergence history

The accuracy of numerical simulations heavily relies on the quality of the computational mesh. In this study, quadrilateral grids were employed, recognizing their suitability for capturing the flow behavior within the cavity. To ensure the robustness and reliability of the results, a thorough grid independence study was conducted. Simulations were performed using three different grid sizes, corresponding to approximately 10,000, 40,000, and 90,000 elements. The grid independence check for the cavity flow is illustrated in Fig. 2, which compares the horizontal velocity variations along the vertical centerline of the cavity for each grid. The

results demonstrate that the differences in solutions between the grids with 40,000 and 90,000 elements are less than 1%, indicating that further refinement beyond this point yields negligible changes in the solution. Consequently, to optimize both simulation time and accuracy, a grid with 40,000 elements was selected for the subsequent simulations, providing a balance between computational cost and solution fidelity.

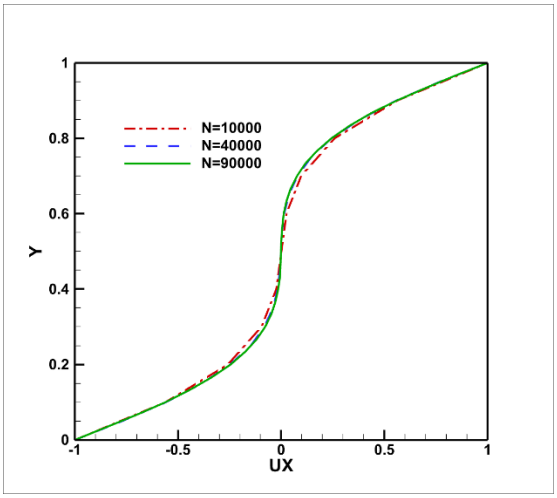

Fig. 2. grid independence (horizontal velocity versus vertical midline of cavity)

To ensure the credibility and reliability of the developed numerical method for cavity flow, a rigorous validation process was undertaken. This involved comparing the simulation results with those reported by Muthtamilselvan et al. [40], a well-established study in the field. The comparison, presented in Table 1, was performed under identical boundary conditions as specified in the work by Muthtamilselvan et al. [40] at a Richardson number (Ri) of 1. Table 1 demonstrates a strong agreement between the present numerical approach and the published data. Specifically, the calculated Nusselt number (Nu) values closely match those reported by Muthtamilselvan et al. [40] for various nano-fluid concentrations (2%, 4%, and 6%). The slight differences observed, such as 2.41 versus 2.40 for C=2%, 2.54 versus 2.56 for C=4%, and 2.76 versus 2.73 for C=6%, are within acceptable limits and can be attributed to minor variations in numerical schemes or grid resolution. This validation confirms that the proposed numerical approach accurately predicts the Nusselt number for different nano-fluid concentrations, thereby establishing its validity and providing confidence in the subsequent results presented in this study. The successful validation underscores the robustness and accuracy of the implemented numerical framework

Table 1
Comparison of average Nu number for cavity flow obtained by the present numerical approach and Muthtamilselvan et al.[40]

	C=2%	C=4%	C=6%
Present work	$\overline{Nu}$ =2.41	$\overline{Nu}$ =2.54	$\overline{Nu}$ =2.76
Muthtamilselvan et al.[40]	$\overline{Nu}$ =2.40	$\overline{Nu}$ =2.56	$\overline{Nu}$ =2.73

Figure 3 illustrates the horizontal velocity contours for free convection at a Richardson number of 10. As evident from the figure, the velocity magnitude is significantly higher in the upper region of the cavity and decreases towards the lower region. This behavior is a direct consequence of the top plate moving to the right and the bottom plate moving to the left. Velocity values near 1 are observed in the upper portion, while values approaching -1 are seen in the lower portion, reflecting the dimensionless nature of the parameters.

Notably, the velocity is close to zero near the left and right sidewalls, as well as along the vertical centerline of the cavity. This indicates regions of reduced flow activity and is consistent with the boundary conditions and the overall flow pattern established by the opposing plate movements. These contours provide a clear visualization of the velocity distribution within the cavity under free convection conditions.

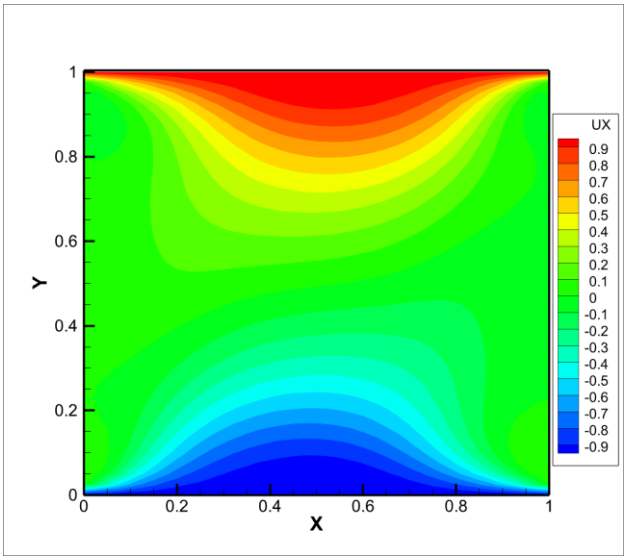

Fig. 3. Horizontal velocity contours at free convection (Ri=10)

Figure 4 presents the vertical velocity contours for free convection at a Richardson number of 10. The vertical velocity varies between 0.85 and -0.85, indicating both upward and downward flow directions. Positive vertical velocity (upward flow) is observed on the left side of the cavity, while negative vertical velocity (downward flow) is present on the right side."

"The minimum vertical velocity, approaching zero, is located in the central region of the cavity. Consistent with the no-slip boundary condition, the vertical velocity is also zero at all four boundaries. A distinct pattern emerges: the velocity begins at zero near the left wall, increases to a maximum value, decreases to near zero at the center, becomes negative, reaches a minimum value, and then increases again to zero at the right wall. This cyclical behavior illustrates the vertical velocity profile within the cavity.

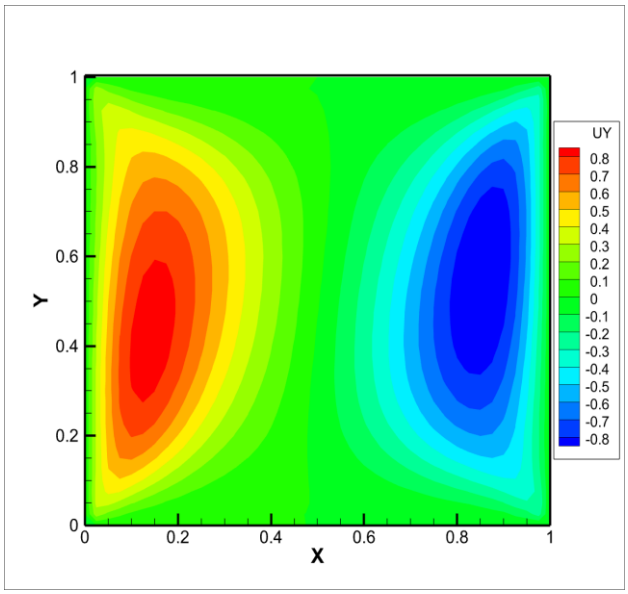

Fig. 4. Vertical velocity contours at free convection (Ri=10)

Figure 5 displays the pressure contours for free convection at a Richardson number of 10. The pressure values range from +13 to -13, although over 90% of the cavity exhibits pressures close to zero. The four corners of the cavity experience significantly higher and lower pressure values.

Specifically, the upper-right and lower-left corners demonstrate positive pressure, while the upper-left and lower-right corners exhibit negative pressure, consistent with the applied boundary conditions. It is important to note that this pressure is relative and dimensionless; therefore, while absolute pressure cannot be negative, the symmetrical distribution reflects the dimensionless nature of the analysis.

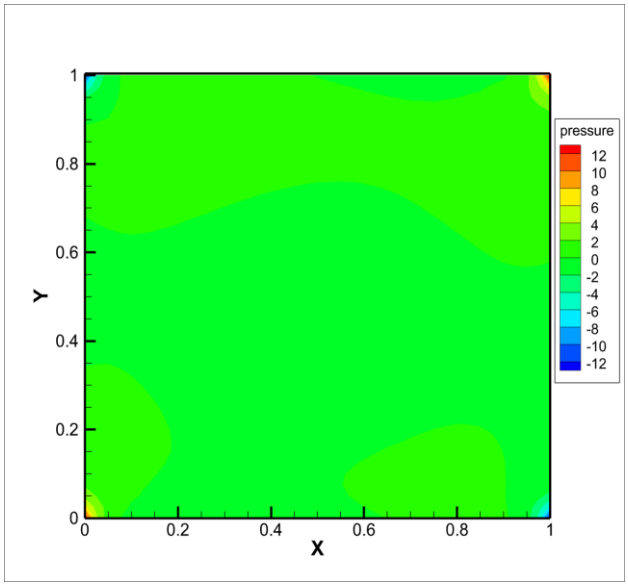

Fig. 5. Pressure contours at free convection (Ri=10)

Figure 6 presents the temperature contours for free convection at a Richardson number of 10. The temperature distribution clearly reflects the imposed boundary conditions, with temperatures approaching +1 near the lower boundary (heated plate) and -1 near the upper boundary (cooled plate). This establishes a strong thermal gradient within the cavity, driving the convective heat transfer process.

The vertical sidewalls, designated as insulated boundaries, are characterized by isotherms that are perpendicular to the wall. This orientation signifies a zero-temperature gradient at these boundaries, indicating no heat flux through the sidewalls. The consistent alignment of the isotherms with the insulated walls provides visual confirmation of the applied boundary conditions and reinforces the validity of the numerical model in accurately representing the physical system.

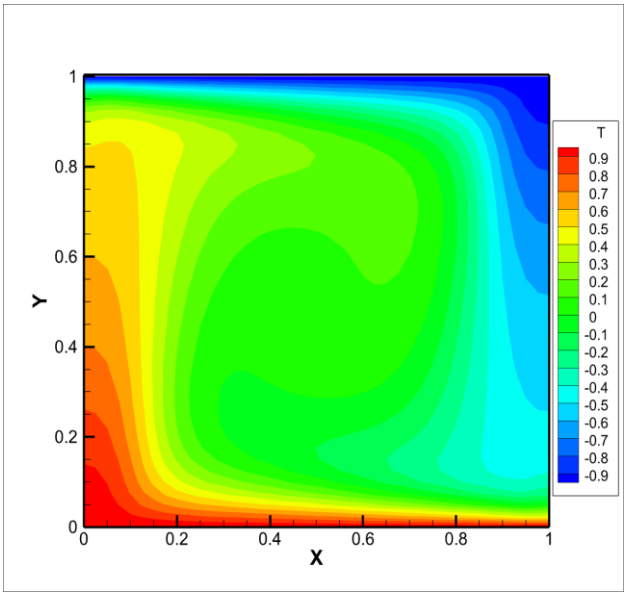

Fig. 6. Temperature contours at free convection (Ri=10)

Figure 7 illustrates the streamlines for free convection at a Richardson number of 10, revealing the complex flow patterns within the cavity. A prominent, large vortex is clearly visible in the central region, indicating a significant rotational flow component. This vortex is a direct consequence of the opposing temperature gradients established by the heated lower plate and the cooled upper plate, leading to a circulating flow pattern.

The streamlines demonstrate a distinct upward flow along the heated left sidewall, converging towards the center of the cavity where they form the core of the vortex.

Subsequently, the flow descends along the right sidewall, completing the circulation loop. It should be noted that although the side walls are adiabatic, the fluid near the right wall experiences lower temperatures as it transitions from the cooled top wall toward the heated bottom wall, maintaining the thermal gradient imposed by the moving and differentially heated boundaries. The density and organization of the streamlines provide valuable insight into the fluid dynamics and heat transfer mechanisms occurring within the cavity under free convection conditions, highlighting the influence of the boundary conditions on the overall flow structure.

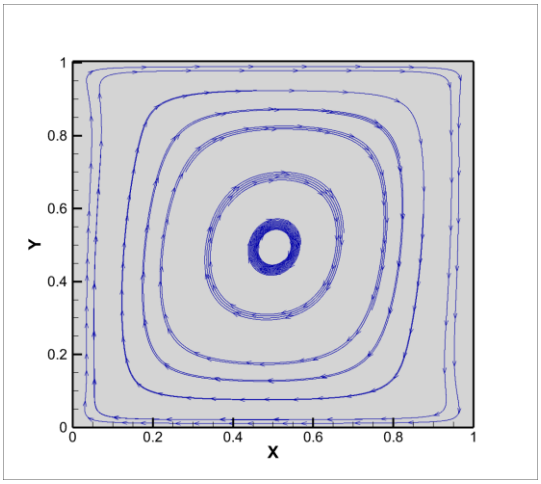

Fig. 7. Streamlines at free convection (Ri=10)

Figure 8 illustrates the variation in Nusselt number for Al_2O_3-water nanofluid and pure water as a function of Richardson number (Ri). The plot reveals a general trend of increasing Nusselt number from left to right, indicating a higher heat transfer rate on the left side of the cavity. Six lines are presented, with three representing pure water and three representing the nanofluid, each corresponding to Ri values of 0.1, 1, and 10, effectively encompassing a range of heat transfer regimes.

The minimum Nusselt number observed is 26, corresponding to pure water at Ri = 0.1. In contrast, the maximum Nusselt number is 32.2, achieved by the nanofluid at Ri = 1. This represents a significant enhancement of approximately 24% in heat transfer when using the nanofluid compared to pure water under these conditions. The simulations were conducted with a Reynolds number of 20 and Grashof numbers of 40, 400, and 4000, ensuring a predominantly convective heat transfer regime.

It is important to note that the location of maximum and minimum Nusselt numbers does not consistently align with the center of the upper cavity boundary due to the intersecting streamlines. This highlights the complex and non-uniform heat transfer distribution within the cavity. Overall, Figure 8 demonstrates the potential of nanofluids to enhance heat transfer in cavity flows, particularly at moderate Richardson numbers.

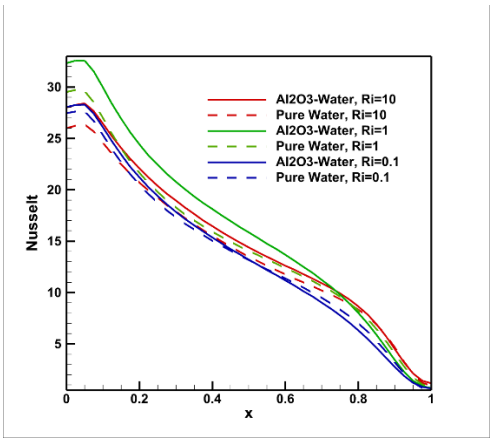

Fig. 8. Nusselt number variation for Al_2O_3-Water and pure water at different Ri

Figure 9 illustrates the variation in friction factor for Al_2O_3-water nanofluid and pure water as a function of position within the cavity at different Richardson numbers (Ri). The friction factor exhibits a distinct pattern, with maximum values observed near the left and right sidewalls, likely attributable to the influence of the solid boundaries. Conversely, the minimum friction factor is found in the central region of the upper cavity surface. A notable difference in friction factor is observed between the nanofluid and pure water. The nanofluid consistently demonstrates a higher friction factor across all Ri values, with an average value of approximately 7.3, compared to 4.0 for pure water. This suggests that the presence of nanoparticles introduces increased viscous drag within the fluid, leading to a higher resistance to flow.

Beyond the sidewalls, the friction factor values for the different Ri conditions vary considerably. The minimum friction factor, approaching zero, is observed for pure water at Ri = 10, while the maximum friction factor is associated with the nanofluid at Ri = 0.1, reaching a value of 1.2. These variations underscore the complex interplay between fluid properties, nanoparticle concentration, and heat transfer conditions in influencing the frictional behavior within the cavity.

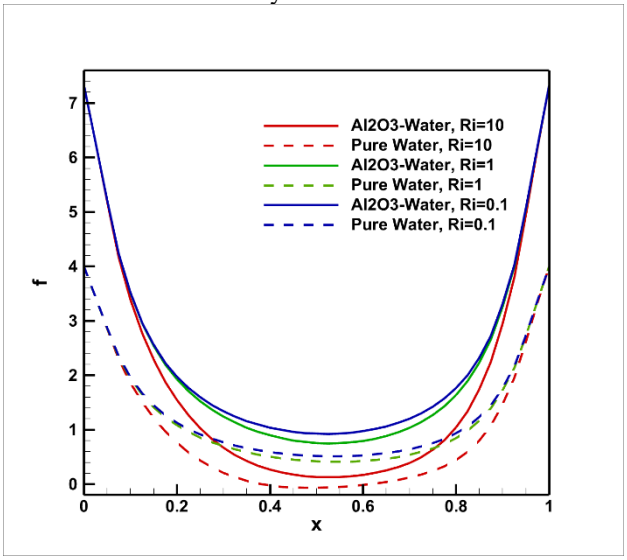

Fig. 9. Friction factor variation for Al_2O_3-Water and pure water at different Ri

The Richardson number (Ri) is defined as the ratio of Grashof number (Gr) to the square of the Reynolds number (Re^2). In this study, the Reynolds number (Re) is maintained constant, while the Grashof number (Gr) is varied to achieve Richardson numbers of 0.1, 1, and 10. An increase in Grashof number, representing a greater temperature difference across the cavity (while maintaining dimensionless boundary temperatures of -1 for the top and +1 for the bottom), signifies a stronger influence of natural convection. The movement of the top and bottom walls introduces forced convection. As the Grashof number increases (leading to higher Ri), the relative contribution of forced convection diminishes compared to the increasingly dominant natural convection effects.

While enhanced heat transfer is a desirable outcome, a comprehensive assessment of the thermo-hydraulic performance in this cavity configuration requires careful consideration of the force required to maintain the motion of the plates. In this scenario, where the bottom plate is heated, the top plate is cooled, and the side walls are insulated, the driving force needed to move the top plate to the right and the bottom plate to the left becomes a critical factor. A configuration that significantly improves heat transfer but necessitates a substantially increased driving force may not be practically feasible. To quantify the net benefit of different configurations, a Performance Evaluation Criterion (PEC) is employed. The PEC is defined as the ratio of the heat transfer enhancement to the force required to maintain plate motion, normalized by a reference case. For scenarios where a constant pumping power (or equivalent force input) is desired, the PEC provides a valuable metric for evaluating the overall efficiency of the system. The PEC is obtained by [41]:

$$TEP = \frac{\frac{Nu}{Nu_0}}{\left(\frac{f}{f_0}\right)^{\frac{1}{3}}} \qquad (6)$$

where Nu is the average Nusselt number for the configuration under consideration, Nu_0 is the average Nusselt number for the reference case, f is the friction factor for the configuration under consideration, and f_0 is the friction factor for the reference case. A PEC value greater than unity indicates that the configuration provides net thermo-hydraulic benefit compared to the reference case.

The table above presents the simulation results of mixed convection (combined forced and natural convection) of Al_2O_3-water nanofluid inside a closed cavity at three different Richardson numbers (Ri = 0.1, 1, and 10). The Richardson number (Ri) represents the ratio of buoyancy forces (natural convection) to inertial forces (forced convection), thus indicating the relative dominance of natural versus forced flow mechanisms. The average Nusselt number (Nu_{av}) and average friction factor (f_{av}) are reported for both the Al_2O_3-water nanofluid and the base fluid (pure water). Finally, the Thermal Efficiency Parameter (TEP) is calculated as a comprehensive metric to evaluate the overall system performance by balancing heat transfer enhancement against the increased pumping power requirement.

- In all cases examined (Ri = 0.1, 1, and 10), the TEP value is less than 1 ,indicating that the enhancement in heat transfer due to the addition of Al_2O_3 nanoparticles is insufficient to compensate for the increased energy consumption caused by higher fluid friction and pumping power.
- At Ri = 0.1 (dominant forced convection regime), the nanofluid shows a marginal improvement in Nu_{av} (13.77 vs. 13.67 for pure water), but this is accompanied by a significant increase in f_{av} (2.39 vs. 1.31). This indicates that the added resistance to flow outweighs the minor gain in heat transfer, resulting in no net benefit in terms of energy efficiency.
- At Ri = 1 (balanced mixed convection), the nanofluid achieves a higher Nu_{av} (16.23 vs. 14.78), suggesting better heat transfer performance. However, this improvement comes at the cost of a substantial rise in f_{av} (2.97 vs. 1.25), which significantly increases the required pumping power. As a result, the TEP decreases to 0.82295, confirming that the energy penalty exceeds the thermal gain.
- At Ri = 10 (dominant natural convection), the heat transfer enhancement of the nanofluid is less pronounced (14.97 vs. 14.06), while the friction factor still increases (1.86 vs. 0.92). Although the TEP improves slightly (0.84205), it remains below unity, indicating that the use of nanofluid does not lead to a net improvement in system efficiency when both heat transfer and flow resistance are considered.

Despite the potential of Al_2O_3-water nanofluids to enhance thermal conductivity and heat transfer ,the results demonstrate that the added pumping power required to overcome increased viscous resistance negates any thermal benefits .Therefore ,the incorporation of nanoparticles into the base fluid does not improve overall system efficiency under the considered conditions , especially when the total energy cost of fluid motion is taken into account. This highlights the importance of evaluating nanofluids not only based on heat transfer enhancement but also on their impact on fluid dynamics and energy consumption in practical applications.

Table 2
PEC for Al_2O_3-Water and Pure Water

	Al_2O_3-Water		Pure Water		
	Nu_{av}	f_{av}	Nu_{av}	f_{av}	TEP
Ri=0.1	13.77	2.39	13.67	1.31	0.82438851
Ri=1	16.23	2.97	14.78	1.25	0.82295193
Ri=10	14.97	1.86	14.06	0.92	0.84205081

4. CONCLUSION

The present numerical study demonstrates that the use of Al2O3–water nanofluid inside a cavity yields nuanced thermofluid performance depending on the convection regime (Ri = 0.1, 1, 10). The main findings are organized to reflect the structure of the manuscript:

Physical Model and Flow Regimes

- Forced convection regime (Ri = 0.1): modest enhancement in Nu with nanofluid (Nu increases from 13.67 to 13.77) but a substantial rise in friction factor (f increases from 1.31 to 2.39), indicating higher pumping power is required.
- Mixed convection (Ri = 1): Nu improves (16.23 vs. 14.78) but with a large friction factor increase (2.97 vs. 1.25), leading to a clear energy penalty. Consequently, the thermo-hydraulic performance deteriorates when considered with pumping costs.
- Natural/convection-dominated regime (Ri = 10): smaller incremental heat transfer gain (Nu ≈ 14.97 vs. 14.06 for base fluid) accompanied by a persistent rise in friction factor (1.86 vs. 0.92), which yields limited or negative net benefits.

Energy Efficiency and Metric Interpretation

- The Thermally Enhanced Performance (TEP) index remains below unity across Ri = 0.1, 1, and 10, with typical values around 0.822–0.84, indicating that the energy penalty from increased viscous resistance generally outweighs the thermal gains.
- Specifically, at Ri = 0.1, the slight Nu improvement does not compensate the higher pumping power, yielding no net energy efficiency gain. At Ri = 1, although Nu is higher, the corresponding pump power demand more than offsets the thermal benefit, giving TEP < 1. At Ri = 10, the marginal heat-transfer enhancement fails to justify the frictional losses, and TEP remains below unity.

Implications for Design and Application

- Across the studied regimes, incorporating Al2O3 nanoparticles in water within the cavity does not improve overall energy efficiency when both heat transfer and pumping power are considered. The observed trends highlight the necessity of evaluating nanofluids with a holistic metric that couples thermal performance to fluid-dynamic penalties.
- The results emphasize that practical design decisions should weigh not only Nu enhancements but also friction-factor penalties and the resulting pumping demands. The potential for optimization exists in selecting targeted Ri ranges or nanoparticle fractions that could yield a net positive effect, but under the present conditions no such improvement is observed.

Validation and Limitations

- Validation against available benchmarks confirms the accuracy of Nu predictions and the reliability of the numerical approach.
- Limitations include the specific nanoparticle volume fraction, particle type (Al2O3), cavity geometry, and boundary conditions. Extensions to other nanofluid compositions, geometries, or transient conditions may alter the conclusion.

Overall Conclusion

Under forced, free, and mixed convection inside a cavity, Al2O3–water nanofluid does not enhance global system efficiency due to the dominant energy cost associated with increased viscous resistance, except for narrowly defined and possibly optimized regimes. The study reinforces the need for comprehensive assessment criteria that integrate heat-transfer performance with energy expenditure in engineering applications.

REFERENCES

[1] Y. Su and X. Lu, "Energy Saving Research on Temperature Control in Data Center Server Rooms," *Journal of Physics: Conference Series,* vol. 2800, no. 1, p. 012033, 2024/07/01 2024, doi: 10.1088/1742-6596/2800/1/012033.

[2] N. V. K, "Opportunities, challenges, and state of the art of flexible heat-pipe heat exchangers: A comprehensive review," *Heat Transfer,* vol. 53, no. 2, pp. 893-938, 2024/03/01 2024, doi: https://doi.org/10.1002/htj.22978.

[3] M. S. Bretado-de los Rios, C. I. Rivera-Solorio, and K. D. P. Nigam, "An overview of sustainability of heat exchangers and solar thermal applications with nanofluids: A review," *Renewable and Sustainable Energy Reviews,* vol. 142, p. 110855, 2021/05/01/ 2021, doi: https://doi.org/10.1016/j.rser.2021.110855.

[4] S. E. Razavi, T. Adibi, S. F. Ahmed, and S. C. Saha, "Semi-analytical solution of nanofluid flow with convective and radiative heat transfer," *International Journal of Modern Physics B,* p. 2450345, 2023, doi: 10.1142/S0217979224503454.

[5] N. Dharmakkan *et al.*, "A case study on analyzing the performance of microplate heat exchanger using nanofluids at different flow rates and temperatures," *Case Studies in Thermal Engineering,* vol. 44, p. 102805, 2023/04/01/ 2023, doi: https://doi.org/10.1016/j.csite.2023.102805.

[6] W. Ajeeb, R. R. S. Thieleke da Silva, and S. M. S. Murshed, "Experimental investigation of heat transfer performance of Al2O3 nanofluids in a compact plate heat exchanger," *Applied Thermal Engineering,* vol. 218, p. 119321, 2023/01/05/ 2023, doi: https://doi.org/10.1016/j.applthermaleng.2022.119321.

[7] T. Adibi, S. E. Razavi, and O. Adibi, "A Characteristic-based Numerical Simulation of Water-titanium Dioxide Nano-fluid in Closed Domains," (in en), *International Journal of Engineering,* vol. 33, no. 1, pp. 158-163, 2020, doi: 10.5829/ije.2020.33.01a.18.

[8] S. Yousefzadeh, H. Rajabi, N. Ghajari, M. M. Sarafraz, O. A. Akbari, and M. Goodarzi, "Numerical investigation of mixed convection heat transfer behavior of nanofluid in a cavity with different heat transfer areas," *Journal of Thermal Analysis and Calorimetry,* vol. 140, no. 6, pp. 2779-2803, 2020.

[9] T. Adibi, S. E. Razavi, O. Adibi, M. Vajdi, and F. Sadegh Moghanlou, "The response of nano-ceramic doped fluids in heat convection models: A characteristics-based numerical approach," (in en), *Scientia Iranica,* vol. 28, no. 5, pp. 2671-2683, 2021, doi: 10.24200/sci.2021.56574.4794.

[10] G. Xia, L. Cao, and G. Bi, "A review on battery thermal management in electric vehicle application," *Journal of Power Sources,* vol. 367, pp. 90-105, 2017/11/01/ 2017, doi: https://doi.org/10.1016/j.jpowsour.2017.09.046.

[11] T. Adibi, S. E. Razavi, S. F. Ahmed, H. Hassanpour, N. Mohammadzadeh, and S. M. Muyeen, "Fluid-Structure-Acoustic coupling analysis for external laminar and turbulent fluid flows," *Results in Physics,* vol. 49, p. 106496, 2023/06/01/ 2023, doi: https://doi.org/10.1016/j.rinp.2023.106496.

[12] M. H. Shojaeefard and S. Saremian, "Analyzing the impact of blade geometrical parameters on energy recovery and efficiency of centrifugal pump as turbine installed in the pressure-reducing station," *Energy,*

vol. 289, p. 130004, 2024/02/15/ 2024, doi: https://doi.org/10.1016/j.energy.2023.130004.

[13] M. W. Azam, G. Q. Chaudhary, U. Sajjad, N. Abbas, and W.-M. Yan, "Performance investigation of solar assisted desiccant integrated Maisotsenko cycle cooler in subtropical climate conditions," *Case Studies in Thermal Engineering,* vol. 44, p. 102864, 2023/04/01/ 2023, doi: https://doi.org/10.1016/j.csite.2023.102864.

[14] A. Elkhatat and S. Al-Muhtaseb, "Climate Change and Energy Security: A Comparative Analysis of the Role of Energy Policies in Advancing Environmental Sustainability," *Energies*, vol. 17, no. 13, doi: 10.3390/en17133179.

[15] X. Li *et al.*, "Artificial intelligence application for assessment/optimization of a cost-efficient energy system: Double-flash geothermal scheme tailored combined heat/power plant," *Energy,* vol. 313, p. 133594, 2024/12/30/ 2024, doi: https://doi.org/10.1016/j.energy.2024.133594.

[16] S. E. Razavi and T. Adibi, "Simulation of fluid flow in a counter-flow heat exchanger with partly elastic intermediate walls," (in en), *Computational Sciences and Engineering,* 2026, doi: 10.22124/cse.2026.32640.1149.

[17] T. Adibi, N. M. Maleki, E. Tavousi, and A. Keshmiri, "Enhancing the heat transfer efficiency in heated tube with a novel multi-twisted blade Turbulators: A numerical analysis," *International Communications in Heat and Mass Transfer,* vol. 169, p. 109717, 2025/12/01/ 2025, doi: https://doi.org/10.1016/j.icheatmasstransfer.2025.109717.

[18] M. I. Afridi, S. Pourahmad, N. M. Maleki, E. Tavousi, A. Rahbari, T. Adibi, and M. Sharifpur, "Experimental examination of thermohydraulic characteristics of a new vibrating rubber tube turbulator with multiple air bubble outlets inserted inside a double-pipe heat exchanger," *International Communications in Heat and Mass Transfer,* vol. 172, p. 110509, 2026/03/01/ 2026, doi: https://doi.org/10.1016/j.icheatmasstransfer.2026.110509.

[19] Ralph L. Webb and N.-H. Kim, *Principles of Enhanced Heat Transfer*. 2007, p. 818.

[20] F. Moghanlou, A. Shams Khorrami, E. Esmaeilzadeh, and H. Aminfar, "Experimental study on electrohydrodynamically induced heat transfer enhancement in a minichannel," *Exp. Therm. Fluid Sci.,* vol. 59, pp. 24–31, 11/01 2014, doi: 10.1016/j.expthermflusci.2014.07.019.

[21] Z. Esmaeili, M. Sheikholeslami, F. Salehi, and H. A. Mohammed, "Simulation of a solar thermal system with a parabolic concentrator incorporating an evacuated tube system equipped with a new designed turbulator and hybrid nanofluid," *Renewable Energy,* vol. 237, p. 121633, 2024/12/01/ 2024, doi: https://doi.org/10.1016/j.renene.2024.121633.

[22] M. Sakkaki, F. Moghanlou, S. Parvizi, H. Baghbanijavid, A. Babapoor, and M. Shahedi Asl, "Phase change materials as quenching media for heat treatment of 42CrMo4 steels," *J. Cent. South Univ.,* vol. 27, pp. 752-761, 02/01 2020, doi: 10.1007/s11771-020-4328-8.

[23] Y. K. Dossumbekov, N. Zhakiyev, M. A. Nazari, M. Salem, and B. Abdikadyr, "Sensitivity analysis and performance prediction of a micro plate heat exchanger by use of intelligent approaches," *International Journal of Thermofluids,* vol. 22, p. 100601, 2024/05/01/ 2024, doi: https://doi.org/10.1016/j.ijft.2024.100601.

[24] R. Li, P. Zhai, J. Li, and X. Liu, "Experimental study and performance enhancement of a novel micro heat pipe photovoltaic/thermal system in a cold region," *Applied Thermal Engineering,* vol. 248, p. 123336, 2024/07/01/ 2024, doi: https://doi.org/10.1016/j.applthermaleng.2024.123336.

[25] M. Moravej, "Efficiency enhancement in a triangular solar flat plate collector by using Al2O3-water nanofluids: An experimental study," (in en), *Challenges in Nano and Micro Scale Science and Technology,* vol. 8, no. 2, pp. 99-108, 2020, doi: 10.22111/tpnms.2020.35575.1197.

[26] D. Lahmer, N. Benamara, H. Ahmad, H. Ameur, and A. Boulenouar, "Combination of the Parallel/Counter Flows Nanofluid Techniques to Improve the Performances of Double-Tube Thermal Exchangers," *Arabian Journal for Science and Engineering,* vol. 47, no. 6, pp. 7789-7796, 2022/06/01 2022, doi: 10.1007/s13369-022-06670-3.

[27] N. S. Pandya, H. Shah, M. Molana, and A. K. Tiwari, "Heat transfer enhancement with nanofluids in plate heat exchangers: A comprehensive review," *European Journal of Mechanics - B/Fluids,* vol. 81, pp. 173-190, 2020/05/01/ 2020, doi: https://doi.org/10.1016/j.euromechflu.2020.02.004.

[28] R. P. Sharma, P. K. Pattnaik, S. R. Mishra, S. Tinker, and S. R. Allipudi, "Enhancing heat transfer on the free convection of conducting hybrid nanofluid through stretching/shrinking surface," *Pramana,* vol. 98, no. 3, p. 96, 2024/07/11 2024, doi: 10.1007/s12043-024-02762-x.

[29] C. M. Mohana and B. R. Kumar, "Numerical and semi-analytical approaches for heat transfer analysis of ternary hybrid nanofluid flow: A comparative study," *Mathematics and Computers in Simulation,* vol. 226, pp. 66-90, 2024/12/01/ 2024, doi: https://doi.org/10.1016/j.matcom.2024.06.019.

[30] P. Shahmohammadi and H. Beiki, "A numerical investigation of γ-Al2O3-water nanofluids heat transfer and pressure drop in a shell and tube heat exchanger," (in en), *Challenges in Nano and Micro Scale Science and Technology,* vol. 4, no. 1, pp. 29-35, 2016, doi: 10.7508/tpnms.2016.01.004.

[31] B. Raei, F. Shahraki, M. Jamialahmadi, and S. M. Peyghambarzadeh, "Experimental investigation on the heat transfer performance and pressure drop characteristics of γ-Al2O3/water nanofluid in a double tube counter flow heat exchanger," (in en), *Challenges*

in Nano and Micro Scale Science and Technology, vol. 5, no. 1, pp. 64-75, 2016, doi: 10.7508/tpnms.2017.01.007.

[32] A. J. Chorin, "A Numerical Method for Solving Incompressible Viscous Flow Problems," *Journal of Computational Physics,* vol. 135, no. 2, pp. 118-125, 8// 1997, doi: http://dx.doi.org/10.1006/jcph.1997.5716.

[33] T. Adibi and S. E. Razavi, "A new characteristic approach for incompressible thermo-flow in Cartesian and non-Cartesian grids," *International Journal for Numerical Methods in Fluids,* vol. 79, no. 8, pp. 371-393, 2015, doi: 10.1002/fld.4053.

[34] S. E. Razavi and T. Adibi, "A novel multidimensional characteristic modeling of incompressible convective heat transfer," *J APPL FLUID MECH,* vol. 9, no. 4, 2016 2016.

[35] T. Adibi, "Three-dimensional characteristic approach for incompressible thermo-flows and influence of artificial compressibility parameter," (in en), *Journal of Computational & Applied Research in Mechanical Engineering (JCARME),* vol. 8, no. 2, pp. 223-234, 02/01 2019, doi: 10.22061/jcarme.2018.2032.1178.

[36] M. Sabour, M. Ghalambaz, and A. Chamkha, "Natural convection of nanofluids in a cavity: criteria for enhancement of nanofluids," *INT. J. NUMER. METHOD H.,* vol. 27, no. 7, pp. 1504-1534, 2017, doi: doi:10.1108/HFF-12-2015-0516.

[37] C. Borgnakke and R. E. Sonntag, "Fundamentals of Thermodynamics," *Don Fowley,* 2015.

[38] T. Adibi, O. Adibi, and S. E. Razavi, "A Characteristic-based Solution of Forced and Free Convection in Closed Domains with Emphasis on Various Fluids," (in en), *International Journal of Engineering,* vol. 32, no. 11, pp. 1689-1695, 2019, doi: 10.5829/ije.2019.32.11b.20.

[39] T. Adibi, Adibi, O. , "Laminar forced convection simulation at different boundary conditions with averaging scheme (numerical and theoretical research," *Mathematical Modelling of Engineering Problems,* vol. 6, no. 4, pp. 519-526, 2019, doi: https://doi.org/10.18280/mmep.060406

[40] M. Muthtamilselvan, P. Kandaswamy, and J. Lee, "Heat transfer enhancement of copper-water nanofluids in a lid-driven enclosure," *Comm. Nonlinear Sci. Numer. Simulat.,* vol. 15, no. 6, pp. 1501-1510, 2010/06/01/ 2010, doi: https://doi.org/10.1016/j.cnsns.2009.06.015.

[41] T. Adibi, S. E. Razavi, S. F. Ahmed, A. Alsharifi, N. A. Shah, and H. Alotaibi, "Optimising heat exchanger efficiency through elastic vortex generators and oscillating walls in pulsating channel flows," *International Journal of Ambient Energy,* vol. 46, no. 1, p. 2529840, 2025/12/31 2025, doi: 10.1080/01430750.2025.2529840.